Energy Advances

ROYAL SOCIETY OF CHEMISTRY

PAPER

View Article Online
View Journal | View Issue



Cite this: *Energy Adv.*, 2022, 1, 385

# Catalytic reduction and reductive functionalisation of carbon dioxide with waste silicon from solar panel as the reducing agent†

Ria Ayu Pramudita,[a] Kaiki Nakao,[ab] Chihiro Nakagawa,[a] Ruopeng Wang,[b] Toshimitsu Mochizuki,[c] Hidetaka Takato,[c] Yuichi Manaka [ac] and Ken Motokura *[ab]

Received 15th December 2021,
Accepted 6th May 2022

DOI: 10.1039/d1ya00077b

rsc.li/energy-advances

$CO_2$ was successfully reduced using powdered waste silicon wafer as a reducing agent and a catalytic amount of tetrabutylammonium fluoride. The waste silicon wafers could be recovered during the production of solar panels or at the end of the product's life cycle. The catalytic reduction reaction occurred under atmospheric pressure of $CO_2$ at 95 °C to produce formic acid at 68% yield based on $CO_2$. The reaction mechanism was investigated based on isotopic experiments and X-ray photoelectron spectroscopy analysis of powdered silicon. This reaction system has potential applications in methanol synthesis and the reductive functionalisation of amine to formamide.

**Broader context**

The reductive conversion of $CO_2$ to useful chemicals is key to the transition to a carbon-neutral economy. Meanwhile, waste solar panels also require proper disposal. Because the reductive transformation of $CO_2$ by silicon-based reducing agent is a well-known catalytic process, here we directly used waste silicon wafers recovered from solar panel production as a reductant for $CO_2$ conversion, without requiring any newly prepared reducing agent. Tetrabutylammnonium fluoride acts as an efficient catalyst for converting $CO_2$ to formic acid with powdered silicon wafer, with a yield up to 68% based on the $CO_2$ used. This reaction system is also applicable to the syntheses of methanol and formamide.

## Introduction

In 2020, the recorded annual mean atmospheric concentration of carbon dioxide ($CO_2$) was 414.01 ppm,[1] almost 50% higher than the average level in the pre-industrial era (278 ppm during 1750–1800).[2] As a consequence, global temperature has risen by approximately 1 °C from the pre-industrial level.[3] Despite a transient reduction of 6.4% of global $CO_2$ emission in 2020 due to various lockdown measures to combat the spread of COVID-19,[4,5] this translates to a mere 0.01 °C reduction in temperature increase by 2050.[6] Moreover, considering the excess $CO_2$ already in the atmosphere, we cannot go back to business-as-usual even after the COVID-19 pandemic is over. The United Nations Environment Programme (UNEP) predicted that a 7.6% annual reduction of $CO_2$ emission for at least a decade is necessary to limit the global temperature rise in 2100 to 1.5 °C above the pre-industrial level.[7] The agency suggested prioritising direct support for zero-emission technologies and infrastructure, reducing fossil fuel subsidies, putting a stop to new coal plants, and promoting nature-based solutions.[6]

The generation of electricity and heat accounts for most of the $CO_2$ emissions[8] when fossil fuels are combusted to release their energy. A major shift to renewable energy would greatly reduce $CO_2$ emission. The year 2020 saw a 7% growth in the use of renewable sources for electricity generation. It is predicted that in 2025, solar photovoltaics (PV) alone would account for 60% of all renewable capacity additions.[9]

On the other hand, using $CO_2$ as a feedstock for chemical processes contributes to the diversification of carbon sources in chemical and energy industries, as well as reduces $CO_2$ emission into the atmosphere.[10–12] However, $CO_2$ is chemically very

[a] *Department of Chemical Science and Engineering, School of Materials and Chemical Technology, Tokyo Institute of Technology, 4259 Nagatsuta-cho, Midori-ku, Yokohama 226-8502, Japan*
[b] *Department of Chemistry and Life Science, Yokohama National University, 79-5 Tokiwadai, Hodogaya-ku, Yokohama 240-8501, Japan. E-mail: motokura-ken-xw@ynu.ac.jp*
[c] *Renewable Energy Research Center, National Institute of Advanced Industrial Science and Technology (AIST), 2-2-9 Machiikedai, Koriyama 963-0298, Japan*

† Electronic supplementary information (ESI) available: Experimental details, XPS spectra, and product data for isotopic experiments. See DOI: https://doi.org/10.1039/d1ya00077b

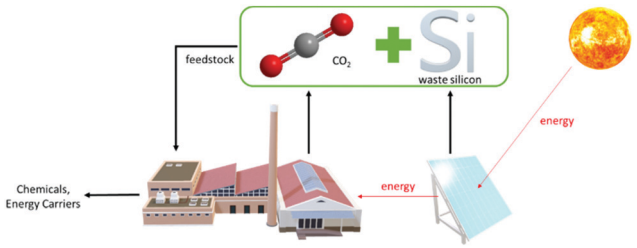


Fig. 1 Potential circular economy when $CO_2$ is reduced by waste silicon from solar panels to produce alternative feedstock for industries.

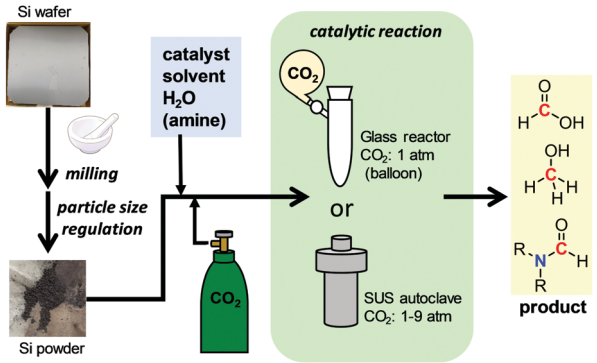


Fig. 2 Method for catalytic $CO_2$ reduction with powdered Si wafer.

stable and therefore not as versatile as hydrocarbons from fossil resources under the current commercially available technology. To overcome this hurdle, it is necessary to increase the energy content of $CO_2$ closer to that of hydrocarbons through a series of chemical reductions, whose cost needs to be competitive against the market price of fossil resources.[13]

One possible cheap reducing agent is metallic silicon, which can be sourced from commercial solar PV cells. The International Renewable Energy Agency (IRENA)[14] estimated that in 2050, there will be 60–78 MT of global PV panel waste, of which two-thirds are of the crystalline silicon variety. The current economic value of these panels is still low,[15] despite the high purity of silicon wafers that account for approximately 2% of their weight.[16] A considerable amount of waste silicon is also produced during the wafer production process. Therefore, utilising waste Si from solar panels to reduce $CO_2$ into organic chemicals and energetic compounds would form a circular economy that is beneficial to the environment, as shown in Fig. 1.

Ozin and coworkers[17] successfully transformed $CO_2$ to CO at a high initial rate of 4.5 mmol $h^{-1}$ $g^{-1}$ Si utilising hydride-terminated silicon nanoparticles at 150 °C and 27 psi (*ca.* 0.2 MPa) and under irradiation of 1 sun solar intensity. Dasog and coworkers[18] synthesised methanol from $CO_2$ (1 MPa) at 150 °C with a methanol yield of 0.23 mmol after 3 h using 0.25 g of hydride-terminated porous silicon nanoparticles. However, in both studies, the silicon powder had to be treated with a large amount of toxic hydrofluoric acid to synthesise the hydride-terminated silicon nanoparticles. Meanwhile, there has been no report on $CO_2$ reduction using real silicon wafer waste from solar panel production.

In this study, we successfully synthesised formic acid, methanol, and formamide from $CO_2$ and powdered silicon wafers obtained from a solar panel production process. This is the first report on catalytic $CO_2$ reduction directly using silicon. A catalytic amount of fluoride salts significantly promoted the reaction under milder reaction conditions (0.1 MPa $CO_2$ pressure, 95 °C). The sources of carbon and hydrogen in formic acid and methanol were confirmed by experiments using $^{13}CO_2$ and $D_2O$, respectively. The key catalytic reaction step is Si–Si bond cleavage and *in situ* formation of an active Si–H species, which was also revealed in the reaction of disilane and $H_2O$ with fluoride.[19–21]

## Methods

The methods for preparing powdered Si wafers and $CO_2$ conversion reactions are summarised in Fig. 2. A silicon wafer used for solar panel production, Czochralski monocrystalline silicon wafer, was obtained from the Renewable Energy Research Center, AIST. It was crushed in an alumina mortar and sifted using an automatic sieve of 300, 90, 40, and 20 μm sizes. To a glass or stainless steel (SUS) autoclave reactor, the powdered wafer, catalyst, solvent, and $H_2O$ were added. Then, $CO_2$ was introduced either by balloon or pressurisation, followed by heating to start the catalytic reaction.

## Results and discussion

The first investigated reaction was the formation of formic acid. As shown in Fig. 3, the effects of catalyst (A), solvent (B), and water additive (C) were screened. Fluoride was found to be the best anion to catalyse this reaction, due to its ability to break the Si–Si bonds in metallic silicon. In the presence of tetrabutylammonium fluoride (TBAF), the amount of formic acid formed was the highest. Tetrabutylammonium (TBA) salts with other anions did not show any catalytic activity. No product was obtained without TBAF catalyst. We also confirmed that no reaction occurred without silicon powder. In terms of solvents, polar aprotic solvents such as dimethylsulfoxide (DMSO), dimethylacetamide (DMA), and *N*-methylpyrrolidone (NMP) were suitable for the reaction, while the less polar ones (toluene and dioxane) performed significantly worse. The reaction was also carried with and without added $H_2O$. Formic acid production was not observed in the absence of $H_2O$, and it reached the optimum value when using 10 mmol of $H_2O$. However, excess $H_2O$ had a detrimental effect on the formic acid yield, probably because of the enhanced solvation effect of TBAF-3$H_2O$, which reduced the activity of fluoride anion as a catalyst.

The effect of silicon particle size was also examined. Fig. 4 shows that the finest powder yielded the most formic acid, which is significantly different from the coarse silicon powders and the parent silicon wafer. Note that Ozin *et al.*[17] utilised silicon nanoparticles with an average diameter of 3.5 nm, and Dasog *et al.*[18] utilised porous silicon nanoparticles with a

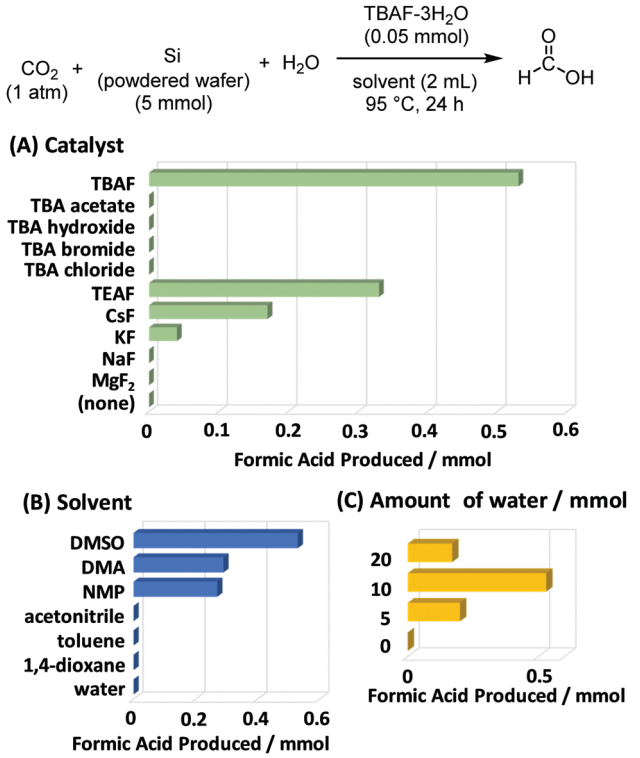


Fig. 3 Effect of (A) catalyst, (B) solvent, and (C) amount of water on the reduction of $CO_2$ with silicon wafer. Basic reaction conditions: powdered silicon wafer (diameter < 40 μm; 5 mmol), $CO_2$ (0.1 MPa, balloon), $H_2O$ (10 mmol), TBAF-$3H_2O$ (0.05 mmol), DMSO (2 mL), 95 °C, 24 h. Yield was determined through internal standard technique of $^1H$ NMR with $CDCl_3$ as the solvent and 1,3,5-triisopropylbenzene as the internal standard.

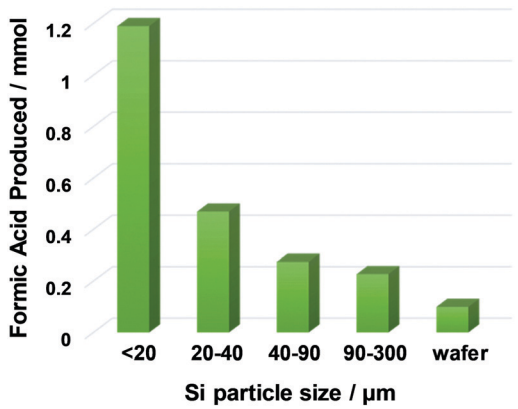


Fig. 4 Effect of silicon particle size on formic acid yield from the reaction system of $CO_2$, $H_2O$, and powdered silicon wafer catalysed by TBAF-$3H_2O$. Reaction conditions: powdered silicon wafer (5 mmol), $CO_2$ (0.1 MPa, balloon), $H_2O$ (10 mmol), TBAF-$3H_2O$ (0.05 mmol), DMSO (2 mL), 95 °C, 24 h. Yield was determined through internal standard technique of $^1H$ NMR with $CDCl_3$ as the solvent and 1,3,5-triisopropylbenzene as the internal standard.

diameter of 155 ± 25 nm. In contrast, the silicon wafers used in this study were only mechanically crushed without any chemical treatment, but they afforded a large amount of formic acid (up to 1.2 mmol) with a catalytic amount of the fluoride source (0.05 mmol). We also examined the reaction using commercially available silicon powder. Under similar conditions using TBAF catalyst, the yield of formic acid was 0.10 mmol,[12] which is much lower than the results reported here. This is due to the particle size differences and/or freshness of silicon particle surface.

The effect of silicon particle size was also apparent from the X-ray photoelectron spectroscopy (XPS) analysis of residual silicon powder after formic acid synthesis, as shown in Table 1 and Fig. S1 (ESI†). Crushing the silicon wafer increased the percentage of exposed $Si^0$ (binding energy, BE: 99.4 eV) on the particle surface, guaranteeing easy access for fluoride anions to break the Si–Si bonds and a high yield of hydrosilane. While most of the $Si^0$ was oxidised to $Si^{4+}$ ($SiO_2$, BE: 103.5 eV) after the reaction, some $Si^0$ remained in the silicon wafer without crash, probably because of the inaccessibility of the inner parts of the wafer to the reagents and catalyst. The fresh silicon powder and recovered solid after the reaction were characterized by XRD and SEM-EDS. As shown in Fig. 5, XRD analysis indicates that clear signals assigned to metallic silicon was observed in fresh powder, while this intensity decreased with increasing a board signal at ~20 degree. This broad signal is assigned to amorphous $SiO_2$. SEM-EDS analysis also revealed that the significant amount of oxygen atom was detected in recovered samples, which was scarcely observed in fresh silicon powder (Fig. S6, ESI†). These results indicate that silicon powder was oxidized by the reduction of $CO_2$.

We have previously reported a reaction mechanism for $CO_2$ reduction by disilane ($R_3Si–SiR_3$) with $H_2O$ and fluoride catalysts, including Si–Si bond cleavage and the *in situ* formation of an active Si–H species that reduces $CO_2$. The applicability of that mechanism to the current reaction system with metallic silicon was examined using isotope experiments, as summarised in Scheme 1. The main goal was to determine whether the formic acid was derived from $CO_2$ and $H_2O$. First, fluoride-catalysed synthesis of formic acid was conducted using an excess amount of $^{13}C$-enriched $CO_2$ (99 atom% $^{13}C$) in a balloon at atmospheric pressure to confirm the source of carbon. The $^1H$ NMR spectrum of the reaction mixture (Fig. S2, ESI†) indicates the coupling of $^{13}C–^1H$ through a split of the formyl peak around 8 ppm with $J_{1H–13C}$ = 215 Hz.[20,23] A similar experiment of formic acid synthesis was performed using 10 mmol of $D_2O$ (>99.8 atom% D) instead of $H_2O$ in typical experiments, in order to confirm the source of proton. After 24 h, the reaction mixture was examined using $^2H$ NMR, where the formic acid-*d* showed a clear peak at 7.82 ppm (Fig. S3, ESI†). Mass analysis also revealed that deuterium was

Table 1 Areal percentage of $Si^{4+}$ and $Si^0$ derived from Si 2p XPS spectra

| Silicon source | Condition | $Si^{4+}$ (%) | $Si^0$ (%) |
|---|---|---|---|
| Si wafer | Fresh | 44 | 56 |
| | After catalysis | 91 | 9 |
| Powdered Si wafer (diameter < 40 μm) | Fresh | 24 | 76 |
| | After catalysis | 99 | 1 |

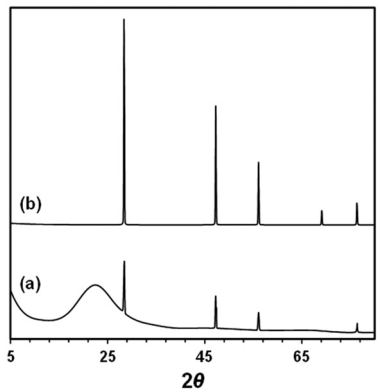


Fig. 5 XRD patterns of (a) recovered solid after catalysis and (b) fresh Si powder.

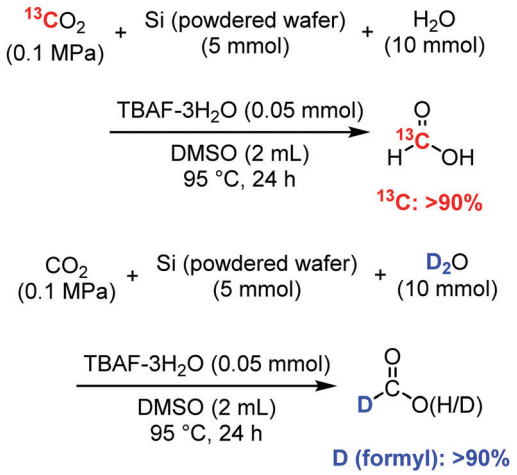


Scheme 1 Isotopic experiment. $^{13}CO_2$: powdered silicon wafer (5 mmol; diameter < 20 μm), $^{13}CO_2$ (1 atm), $H_2O$ (10 mmol), TBAF-$3H_2O$ (0.05 mmol), DMSO (2 mL), 95 °C, 24 h. $D_2O$: powdered silicon wafer (5 mmol; diameter < 20 μm), $CO_2$ (1 atm, balloon), $D_2O$ (10 mmol), TBAF-$3H_2O$ (0.05 mmol), DMSO (2 mL), 95 °C, 24 h.

Table 2 Catalytic high-yield synthesis of formic acid from $CO_2$ and powdered silicon wafer[a]

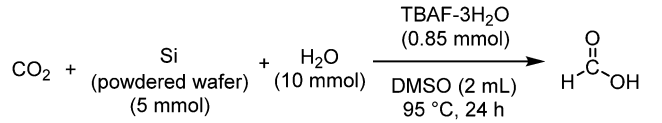


| Reactor | $CO_2$[b] (atm) | Formic acid[c] (mmol) | Yield of formic acid based on $CO_2$[d] (%) |
|---|---|---|---|
| Glass (balloon) | 1.0 (excess) | 0.55 | — |
| Autoclave | 1.0 | 0.82 | 68 |
| Autoclave | 3.0 | 1.03 | 28 |
| Autoclave | 5.0 | 1.05 | 17 |
| Autoclave | 9.2 | 1.75 | 16 |

[a] Reaction conditions: powdered silicon wafer (5 mmol; diameter < 20 μm), $CO_2$, $H_2O$ (10 mmol), catalyst (0.85 mmol), DMSO (2 mL), 95 °C, 24 h. [b] Initial pressure during $CO_2$ introduction. [c] Yield was determined using the internal standard technique of $^1H$ NMR with $CDCl_3$ as the solvent and 1,3,5-triisopropylbenzene as the internal standard. [d] Yield was calculated based on the amount of $CO_2$ used.

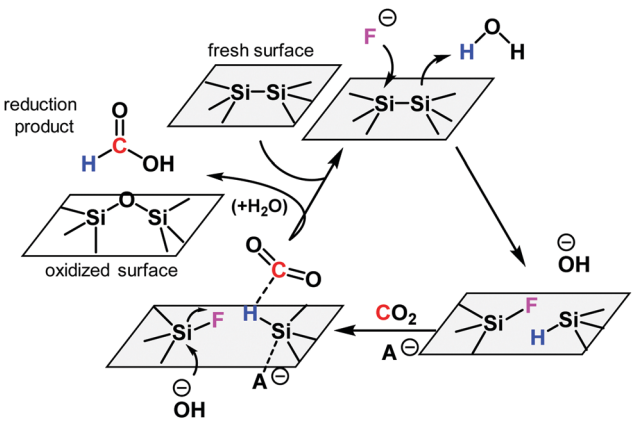


Scheme 2 Proposed catalytic reaction mechanism. $A^-$: fluoride or hydroxide ion.

incorporated into the formyl group of the synthesised formic acid (Fig. S4, ESI†).

To increase the conversion of $CO_2$, we further optimised the reactor and $CO_2$ pressure, as shown in Table 2. The use of an SUS autoclave reactor with a volume of 27 mL and atmospheric pressure of $CO_2$ significantly increased the yield of formic acid to 68% (based on $CO_2$). Meanwhile, the amount of formic acid increased continuously with increasing $CO_2$ pressure.

To understand the mechanism of $CO_2$ reduction reaction with the powdered silicon wafer, F 1s XPS spectra were measured for the silicon wafer and the catalyst as shown in Fig. S5 (ESI†). After the reaction, silicon bonded with one or two fluorine atoms. The formation of Si–H on the silicon surface in the presence of fluoride and $H_2O$ is widely accepted.[17,18] The isotopic experimental results in Scheme 1 indicate that $CO_2$ and $H_2O$ are converted to formic acid. Considering these findings, we propose a reaction mechanism (Scheme 2) for the fluoride-catalysed reduction of $CO_2$ by metallic silicon and $H_2O$. Initially, fluoride anions attack and cleave Si–Si bonds near the surface. A new Si–F bond is formed in the silicon that is more electron-deficient, and the other silicon atom forms a new Si–H bond with nearby water molecule. The newly formed Si–H bond reduces $CO_2$ with the help of an anionic catalyst ($A^-$: fluoride or hydroxide) according to a previously reported mechanism.[22] The resulting surface-bonded silylformate then undergoes hydrolysis to yield formic acid and an oxidised surface. Because of the high oxophilicity of silicon atoms, some of the Si–F is replaced by silanols (Si–OH) or siloxane (Si–O–Si), and a free fluoride anion is regenerated. However, the replacement of fluorosilane with silanol may not be irreversible but rather follows an equilibrium.[20] This reaction mechanism is based on the reaction between $CO_2$, $H_2O$, and disilane ($R_3Si$–$SiR_3$).[22]

The TBA-catalysed reaction system using the powdered silicon is potentially applicable to produce other reduction

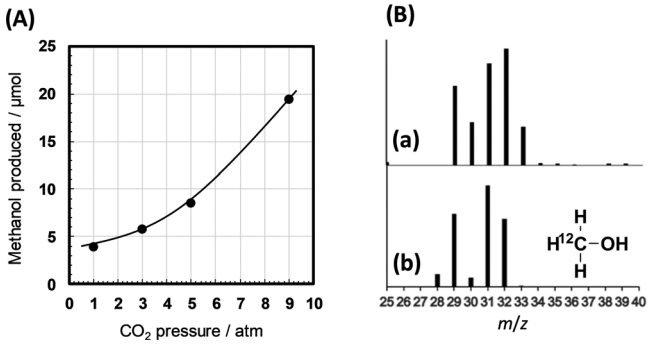


Fig. 6 (A) Effect of $CO_2$ pressure on the methanol yield. Reaction conditions: powdered silicon wafer (5 mmol; diameter < 20 μm), $CO_2$, $H_2O$ (10 mmol), TBAF-$3H_2O$ (0.85 mmol), DMSO (2 mL), 95 °C, 24 h. Yield was determined by GC-FID using an internal standard technique. (B) Mass spectra of methanol produced in the reactions using (a) $^{13}CO_2$ and (b) $^{12}CO_2$.

products from $CO_2$. During the isotopic experiments investigating the carbon and hydrogen sources of formic acid (Scheme 1), we observed methanol, a six-electron reduction product of $CO_2$, in our reaction mixture. The methanol yield increased with increasing $CO_2$ pressure (Fig. 6A). In addition, this methanol contains a considerable amount of $^{13}C$ (Fig. 6B), meaning that it originates from $CO_2$ by reduction with hydride from $H_2O$. Further optimisation of the reaction conditions may increase the methanol yield.

Another important application of our powdered silicon-TBAF catalytic system is the reductive functionalisation of $CO_2$. In the presence of morpholine, both $CO_2$ reduction and C–N bond formation proceeded to produce *N*-formyl morpholine with a 87% yield (Scheme 3). Isotopic experiments using $^{13}CO_2$ and $D_2O$ indicated that the formyl group of the product was derived from $CO_2$ and $H_2O$. No formylation product was obtained in the absence of powdered Si. The use of hydrosilane or molecular hydrogen for reductive functionalisation is well known.[23] However, this is the first report on reductive functionalisation using powdered Si wafer, a waste material, as the reducing agent.

## Conclusions

We have shown that metallic silicon waste recovered from the solar panel production process can be utilised as a reducing agent for $CO_2$ to produce formic acid, methanol, and formamide. We demonstrated that fluoride compounds such as TBAF act as efficient catalysts for the reductive transformation of $CO_2$, with up to 68% yield of formic acid. Isotopic experiments and XPS analysis of silicon before and after the catalytic reaction revealed that the fluoride-silicon interaction induced the *in situ* formation of Si–H species, which in turn reduced $CO_2$. This is the first report of a catalytic $CO_2$ reduction process that directly uses waste metallic silicon. This methodology has the potential to achieve the dual goals of recycling $CO_2$ as a chemical feedstock and utilising silicon waste from solar panels to produce energy storage materials.

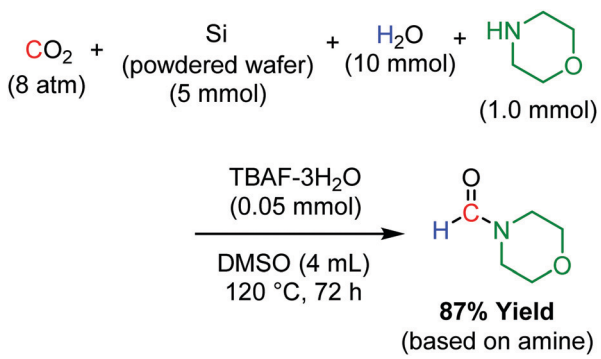


Scheme 3 Reductive functionalisation of $CO_2$ with an amine.

## Author contributions

K. M. and R. A. P. conceived and supervised the project. K. N. and C. N. conducted most of the experiments and analysed the data. R. W. performed the formamide synthesis experiments. T. M. and H. T. prepared metallic Si. Y. M. conceived the catalytic $CO_2$ conversion mechanism and supervised its study. R. A. P. and K. M. wrote the manuscript.

## Conflicts of interest

There are no conflicts to declare.

## Acknowledgements

Part of this study was supported by the JSPS Grant-in-Aid for Scientific Research on Innovative Areas (grant no. JP20H04804) and Transformative Research Areas (grant no. JP21H05099), the Noguchi Institute, and the Yazaki Memorial Foundation for Science and Technology.

## Notes and references

1 The Meteorological Office, UK, "Mauna Loa carbon dioxide forecast for 2021," can be found under https://www.metoffice.gov.uk/research/climate/seasonal-to-decadal/long-range/forecasts/co2-forecast.
2 C. M. Meure, D. Etheridge, C. Trudinger, P. Steele, R. Langenfelds, T. van Ommen, A. Smith and J. Elkins, *Geophys. Res. Lett.*, 2006, **33**, L14810.
3 NOAA National Centers for Environmental Information, State of the Climate: Global Climate Report for Annual 2020, NOAA National Centers For Environmental Information, 2021.
4 J. Tollefson, *Nature*, 2021, **589**, 343.
5 Z. Liu, P. Ciais, Z. Deng, R. Lei, S. J. Davis, S. Feng, B. Zheng, D. Cui, X. Dou, B. Zhu, R. Guo, P. Ke, T. Sun, C. Lu, P. He, Y. Wang, X. Yue, Y. Wang, Y. Lei, H. Zhou, Z. Cai, Y. Wu, R. Guo, T. Han, J. Xue, O. Boucher, E. Boucher, F. Chevallier, K. Tanaka, Y. Wei, H. Zhong, C. Kang, N. Zhang, B. Chen, F. Xi, M. Liu, F.-M. Bréon, Y. Lu, Q. Zhang, D. Guan,

P. Gong, D. M. Kammen, K. He and H. J. Schellnhuber, *Nat. Commun.*, 2020, **11**, 5172.
6 United Nations Environment Programme, ''Emissions Gap Report 2020,'' can be found under **https://www.unenvironment.org/emissions-gap-report-2020**, 2020.
7 United Nations Environment Programme, Emissions Gap Report 2019, Nairobi, Kenya, 2019.
8 International Energy Agency, ''Data & Statistics,'' can be found under **https://www.iea.org/data-and-statistics**, n.d.
9 International Energy Agency, Renewables 2020: Analysis and Forecast to 2025, International Energy Agency, 2020.
10 M. Aresta, *Carbon Dioxide as Chemical Feedstock*, John Wiley & Sons, Ltd, 2010, pp. 1–13.
11 W.-H. Wang, X. Feng and M. Bao, in *Transformation of Carbon Dioxide to Formic Acid and Methanol*, ed. W.-H. Wang, X. Feng and M. Bao, Springer, Singapore, 2018, pp. 1–6.
12 T. Sakakura, J.-C. Choi and H. Yasuda, *Chem. Rev.*, 2007, **107**, 2365–2387.
13 P. De Luna, C. Hahn, D. Higgins, S. A. Jaffer, T. F. Jaramillo and E. H. Sargent, *Science*, 2019, **364**, 350.
14 S. Weckend, A. Wade and G. A. Heath, *End of Life Management: Solar Photovoltaic Panels*, IRENA And IEA-PVPS, 2016.
15 O. Tomioka, ''Japan tries to chip away at mountain of disused solar panels – Nikkei Asian Review,'' can be found under **https://asia.nikkei.com/Business/Technology/Japan-tries-to-chip-away-at-mountain-of-disused-solar-panels**, 2016.
16 Study group on reuse, recycling, and proper disposal of used renewable energy equipment, Report on reuse, recycling, and proper disposal of solar power generation equipments, Japan's Ministry Of The Environment, 2016.
17 W. Sun, C. Qian, L. He, K. K. Ghuman, A. P.-Y. Wong, J. Jia, A. A. Jelle, P. G. O'Brien, L. M. Reyes, T. E. Wood, A. S. Helmy, C. A. Mims, C. V. Singh and G. A. Ozin, *Nat. Commun.*, 2016, **7**, 12553.
18 M. Dasog, S. Kraus, R. Sinelnikov, J. G.-C. Veinot and B. Rieger, *Chem. Commun.*, 2017, **53**, 3114–3117.
19 K. Motokura, M. Naijo, S. Yamaguchi, A. Miyaji and T. Baba, *Chem. Lett.*, 2015, **44**, 1464–1466.
20 K. Motokura, M. Naijo, S. Yamaguchi, A. Miyaji and T. Baba, *Chin. J. Catal.*, 2017, **38**, 434–439.
21 K. Motokura and R. A. Pramudita, *Chem. Rec.*, 2019, **19**, 1199–1209.
22 K. Motokura, M. Naijo, S. Yamaguchi, A. Miyaji and T. Baba, *Chem. Lett.*, 2015, **44**, 1217–1219.
23 Q. Liu, L. Wu, R. Jackstell and M. Beller, *Nat. Commun.*, 2015, **6**, 1–15; G. Fiorani, W. Guo and A. W. Kleij, *Green Chem.*, 2015, **17**, 1375–1389; X.-F. Liu, R. Ma, C. Qiao, H. Cao and L.-N. He, *Chem. – Eur. J.*, 2016, **22**, 16489–16493; F. D. Bobbink, S. Das and P. J. Dyson, *Nat. Protoc.*, 2017, **12**, 417–428; X.-Y. Li, S.-S. Zheng, X.-F. Liu, Z.-W. Yang, T.-Y. Tan, A. Yu and L.-N. He, *ACS Sustainable Chem. Eng.*, 2018, **6**, 8130–8135; R. A. Pramudita and K. Motokura, *Green Chem.*, 2018, **20**, 4834–4843; R. A. Pramudita and K. Motokura, *ChemSusChem*, 2021, **14**, 281–292.